Analysis of ^{6}Li+^{16}O elastic scattering using different potentials

Sh. Hamada[a], B. Alshahrani[b], Abd Elrahman Elgamala[a], N. Darwish[a], I. Bondouk[a] and Awad A. Ibraheem[b,c]

[a]*Faculty of Science, Tanta University, Tanta, Egypt*
[b]*Physics Department, King Khalid University, Abha, Saudi Arabia*
[c]*Physics Department, Al-Azhar University, Assiut Branch, Assiut 71524, Egypt*
sh.m.hamada@science.tanta.edu.eg; awad_ah_eb@hotmail.com

Elastic scattering of ^{6}Li from ^{16}O nucleus in the energy range of $13.0 - 50.0$ MeV was analyzed within the framework of optical potential, double folding optical potential, and cluster folding potentials. The present study involves theoretical calculations based on available experimental angular distributions of the scattering process. Of particular interest is the cluster folding based on the well-known cluster structure of ^{6}Li. Elastic scattering data for the ^{6}Li+^{16}O system plotted as a function of momentum transfer showed that the real Coulomb nuclear interference region is independent of the bombarding energy. This structural pattern could be used to define the interaction potential with some certainty and to extract reliable values for the renormalization factors.

Keywords: Elastic scattering; folding potential; cluster folding.

1. Introduction

Lithium nucleus is considered as one of the most interesting and widely used nuclei in lithium-induced nuclear reactions and scattering processes on various targets. One reason could be attributed to the well-known cluster structure of ^{6}Li consisting of a core (α-alpha) and a valence (d-deuteron) orbiting the core. In the past decades, lithium scattering angular distributions have been available for a variety of targets and beam energies. There are several studies to reproduce the experimental angular distribution measurements using the phenomenological Woods-Saxon (WS) optical potential as well as double folding (DF) potentials [1-12]. The energy dependency of ^{6}Li+^{16}O was performed by Rudchik *et al.* [11], and the data on the effect of nucleus-nucleus interaction were obtained from the internal structure of the colliding nucleus. The general inferences based on the previous works on the lithium elastic scattering of different targets (including ^{16}O nucleus) are: a) the capability of the optical model to reproduce the experimental data over a wide range of bombarding energies, b) Appreciable deviations generally occur for backward angles, c) For a given reaction, the potential parameters are either constant or change smoothly with bombarding energy, d) The observed discrete ambiguities of the families of potential parameters cannot be experimentally reduced unless data at higher bombarding energies are available, and e) Spin-orbit effects do not play a significant role.

Poling *et al.* [1] analyzed the angular distributions for ^{6}Li+^{12}C and ^{7}Li+^{12}C elastic scattering at beam energies ranging from 4.5 to 13.0 MeV using optical potentials of four varying parameters, with the imaginary potential depth varying linearly with energy. In another phenomenological study, Bindal *et al.* [2] analyzed ^{6}Li+^{12}C elastic scattering at energies greater than 20.0 MeV using optical potentials of six varying parameters, where both the real and imaginary potential depths varied linearly with energy. Poling *et al.* [3] mea-

sured and analyzed the angular distributions for ^{6}Li and ^{7}Li elastically scattered from ^{10}B, ^{12}C, ^{13}C, ^{16}O, and ^{28}Si at energies between 4.0 and 13.0 MeV. The experimental data for the different nuclear systems considered in this study were reproduced using the optical model (OM). In certain cases, the back angles were not well fitted by parameter sets, which were otherwise useful for all energies. The effects of compound nucleus formation are hypothesized to be the cause of rapid energy variations in the angular distributions. Vineyard *et al.* [13] and Trcka *et al.* [14] measured and analyzed the angular distributions for ^{6}Li+^{16}O system at energies 25.7 and 50.0 MeV. The data were analyzed using both OM and double folded potentials with renormalization factors 0.61 and 0.65 at energies 25.7 and 50.0 MeV, respectively. In other words, the potentials were to be reduced in strength by about 37% to reproduce the data.

This paper is organized as follows. In Sec. 2, the theoretical calculations based on the experimental data are presented. Section 3 is devoted to the results of the theoretical analysis and discussions. The summary is given in Sec. 4.

2. Theoretical calculations

The angular distributions for ^{6}Li+^{16}O elastic scattering in the energy range of $13.0 - 50.0$ MeV are reanalyzed using different phenomenological and semi-microscopic potentials such as optical potential (OP), double folding (DF), and cluster folding (CF) potentials. Firstly, the elastic scattering data for ^{6}Li+^{16}O at energies 13.0 MeV [3], 20.0 MeV [5], 25.7 MeV [13], 30.0 MeV [15], 32.0 MeV [16], 36.0 MeV [17], 48.0 MeV [18], and 50.0 MeV [14] are investigated within the framework of OM. The parameters defined by Trcka *et al.* [14] are taken as starting parameters. The analysis employed real and imaginary volume central potentials together with Coulomb potential. The spin-orbit interaction for ^{6}Li has a

little influence on the differential cross-section, thus it was not considered. The used potential has the following form:

$$U(R) = V_c(r) - Vf(r, r_V, a_V) - iWf(r, r_W, a_W) \quad (1)$$

where $f(r, r_x, a_x)$, $x = V$, W is the Woods-Saxon form factor which equals to $[1 + \exp[(r - r_x A^{1/3})/a_x]]^{-1}$ and $V_c(r)$ is the Coulomb potential caused by a uniform sphere with a charge equal to that of the target nucleus and radius $r_c A_t^{1/3}$. Two parameters "r_V and r_W" were fixed during the search to the values 1.37 and 1.88 fm, respectively, and the rest four parameters V_0, a_V, W_0, and a_W were allowed to be changed freely to minimize χ^2, defined by:

$$\chi^2 = \frac{1}{N} \sum_{i=1}^{N} \left(\frac{\sigma(\theta_i)^{\text{cal}} - \sigma(\theta_i)^{\text{exp}}}{\Delta\sigma(\theta_i)} \right)^2, \quad (2)$$

where N is the number of experimental data points $\sigma(\theta_i)^{\text{cal}}$ and $\sigma(\theta_i)^{\text{exp}}$ are the calculated and experimental cross-sections, $\Delta\sigma(\theta_i)$ is the uncertainty of the data. By employing this technique, we could obtain an energy dependence on both real and imaginary potential depths. All the calculations in the present work were performed using the code FRESCO [19], and SFRESCO search code was used in searching for the optimal potential parameters. The Coulomb radius parameter was taken as a fixed value at 2.3 fm in all calculations.

Secondly, the available data sets for ^{6}Li+^{16}O angular distributions were analyzed using the double folding optical model (DFOM). In this model, the real part of the interaction potential was derived based on DF, where ^{6}Li and ^{16}O densities in their ground states are folded to nucleon-nucleon potential using the code DFMSPH [20]. The real part of the potential is calculated from the equation given below:

$$V_{DF}(R) = \iint \rho_P(r_1)\rho_T(r_2)v_{nn}(S)d\vec{r_1}d\vec{r_2} \quad (3)$$

where $v_{nn}(S)$ is the effective nucleon-nucleon interaction with $S = |\vec{R} - \vec{r_1} + \vec{r_2}|$ which is the distance between the two nucleons. The effective $v_{nn}(S)$ interaction potential was taken to be of the CDM3Y6 [21]. The density distribution of ^{16}O is expressed in a modified form of the Gaussian shape as: $\rho(r) = \rho_0(1 + wr^2)\exp(-\beta r^2)$, where $\rho_0 = 0.1317$, $w = 0.6457$ and $\beta = 0.3228$ [22]. The density distribution of ^{6}Li nucleus is taken from earlier work [23] as follow:

$$\rho(r) = 0.203 \exp(-0.3306r^2) + \lfloor -0.0131 + 0.001378r^2 \rfloor$$
$$\times \exp(-0.1584r^2) \quad (4)$$

The imaginary part of the potential was taken in the Woods-Saxon shape; the optimal imaginary potential parameters obtained from OM calculations were taken as it is in the DFOM calculations, and consequently, only one variable parameter N_R "renormalization factor for the real part of the potential" was used in the calculations. The nuclear potential, in this case, has the following shape:

$$U(R) = V_c(r) - N_R V_{DF}(r) - iWf(r, r_w, a_w) \quad (5)$$

Thirdly, motivated by the well-known $d+\alpha$ cluster structure of ^{6}Li, the existing experimental data for ^{6}Li+^{16}O elastic scattering in the energy range of $13.0 - 50.0$ MeV were analyzed using the CF model potential as the basis. The basic ingredients needed to calculate the CF potential for ^{6}Li+^{16}O system are $d + \alpha$ binding potential, required to calculate the wave function for the relative motion of the d and α in ^{6}Li, and $d + ^{16}$O and $\alpha + ^{16}$O optical potentials, obtained by fitting the respective elastic scattering data for nearly the same value of E/A for the data of interest. The $d+^{16}$O and $\alpha+^{16}$O optical potentials were taken from the literature [24,25]. The bound-state wave function for the relative motion of d and α in the cluster plus core configuration in ^{6}Li represents a $2S$ state in a real Woods-Saxon potential with a fixed radius $r = 1.15$ and diffuseness $a = 0.65$ fm. The potential depth was adjusted to reproduce the binding energy of 1.4737 MeV
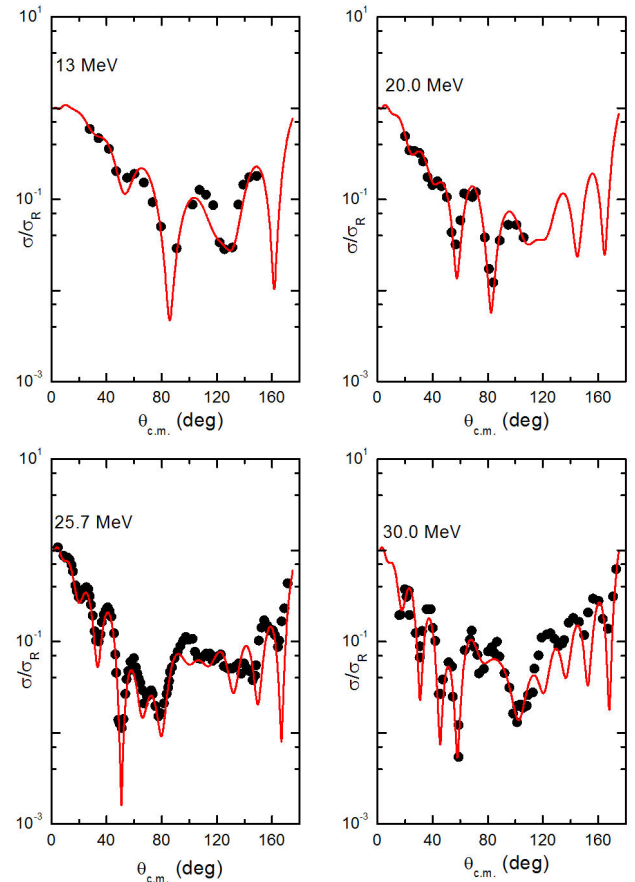

FIGURE 1. Comparison between experimental angular distributions (solid black circles) for ^{6}Li + ^{16}O elastic scattering and the theoretical calculations (solid red curves) using OM at $E_{lab} = 13.0, 20.0, 25.7,$ and 30.0 MeV.
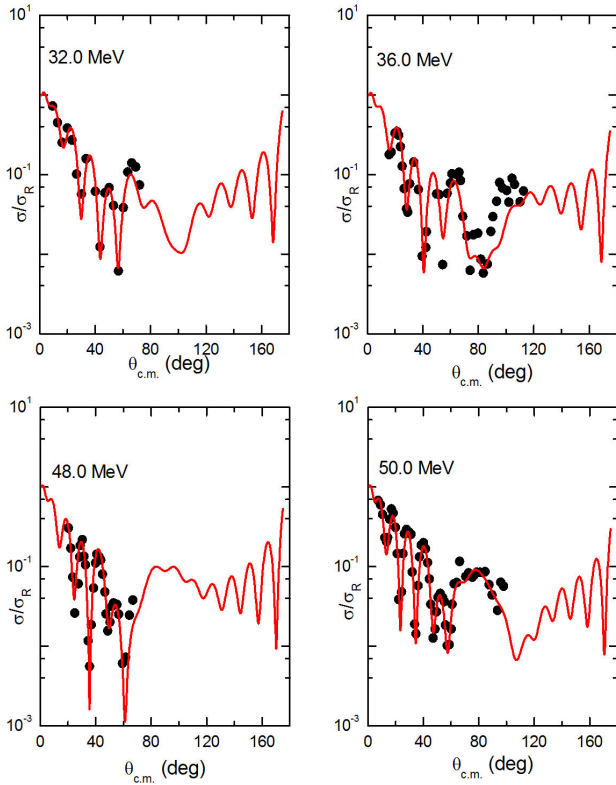
FIGURE 2. Comparison between experimental angular distributions (solid black circles) for ^{6}Li + ^{16}O elastic scattering and the theoretical calculations (solid red curves) using OM at E_{lab} = 32.0, 36.0, 48.0, and 50.0 MeV.

of the cluster. Both the real and imaginary parts of these potentials were then folded over the cluster wave function to produce the ^{6}Li+^{16}O CF potential.

3. Results and discussion

One of the aims of the current study was to investigate the energy dependence of ^{6}Li scattering from ^{16}O to obtain energy-dependent optical potentials and global optical potential parameters for the ^{6}Li + ^{16}O system. In the last few years, more data have become available on energy dependence, and the upper energy limit has extended. The old energy-dependent optical potentials are not adequate to produce correct data, particularly, at large angles, and high energies. Thus, there is a need for improved average optical potentials for this nuclear system. We performed an (OM) analysis for the ^{6}Li + ^{16}O elastic scattering angular distributions in the energy range of $13.0 - 50.0$ MeV using pure phenomenological Woods-Saxon potentials for both real and imaginary volume parts. The comparisons between the experimental data at energies (13.0, 20.0, 25.7, 30.0, 32.0, 36.0, 48.0, and 50.0 MeV) and the theoretical calculations using OM are shown in Figs. 1-2. The optimal extracted potential parameters are listed in Table I.

We have investigated the energy dependence on the values V_0 and W_0 for the ^{6}Li + ^{16}O system, as shown in Fig. 3 and can be approximated by: V_0 (MeV) $= 183.06 + 0.0346E$ (MeV), and W_0 (MeV) $= 5.035 + 0.218E$ (MeV). The available experimental data for ^{6}Li+^{16}O are then analyzed within the framework of DFOM; the data were fitted using only one parameter "N_R" while the imaginary phenomenological potential parameters were taken the same as those obtained from OM calculations. The comparisons between the experimental angular distributions data for ^{6}Li + ^{16}O nuclear system at the different concerned energies and theoretical calculations using this model are shown in Figs. 4-5. It is clear that using such hard constraints, the quality of fitting got worse "see the values of χ^2/N extracted from the OM and DFOM calculations". The data analysis using DFOM showed and emphasized the necessity for reduction N_R by about 40%. The optimal potential parameters used in the DFOM calculations are listed in Table II.

The elastic scattering data for ^{6}Li + ^{16}O system plotted as a function of momentum transfer (Fig. 6) showed that the interference peaks and valleys line up whereas, if we plotted the data as a function of angle there is no apparent pattern.

TABLE I. Global optical potential parameters for ^{6}Li + ^{16}O nuclear system extracted from the OM analysis, the values of reaction cross-sections σ_R as well as real J_V and imaginary J_W volume integrals are also listed.

E	V_0	r_V	a_V	W_0	r_W	a_W	χ^2/N	σ_R	J_V	J_W
(MeV)	(MeV)	(fm)	(fm)	(MeV)	(fm)	(fm)		(mb)	(MeV.fm^3)	(MeV.fm^3)
13.0	186.01	1.37	0.719	7.14	1.88	0.949	7.4	1183	477.0	46.3
20.0	185.87	1.37	0.666	9.11	1.88	0.93	8.1	1288	456.3	58.3
25.7	183.13	1.37	0.716	11.23	1.88	0.93	11.5	1438	468.5	71.9
30.0	180.06	1.37	0.734	11.65	1.88	0.93	16.6	1477	467.6	74.6
32.0	182.15	1.37	0.721	12.59	1.88	0.93	7.5	1496	467.9	80.6
36.0	182.46	1.37	0.701	13.64	1.88	0.93	17.9	1513	460.9	87.4
48.0	188.0	1.37	0.664	14.09	1.88	0.95	16.8	1530	460.8	91.3
50.0	185.6	1.37	0.708	16.25	1.88	0.862	5.2	1439	471.6	100.0

TABLE II. Potential parameters for the ^{6}Li + ^{16}O system extracted from the DFOM analysis, the values (σ_R, J_V and J_W) are also listed.

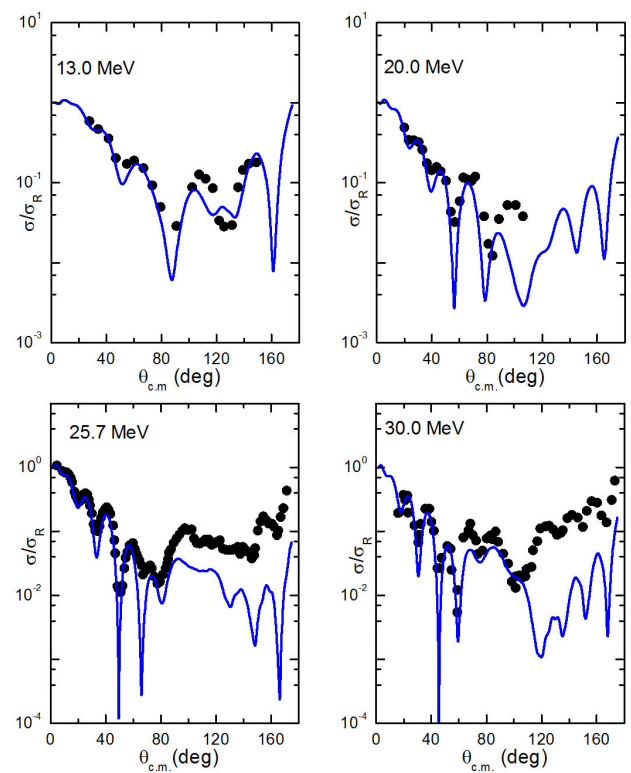| E	N_R	W_0	r_W	a_W	χ^2/N	σ_R	J_V	J_W
(MeV)		(MeV)	(fm)	(fm)		(mb)	(MeV.fm^3)	(MeV.fm^3)
13.0	0.795	7.14	1.88	0.949	12.7	1237	403.9	46.3
20.0	0.584	9.11	1.88	0.93 2	4.3	1354	293.7	58.3
25.7	0.584	11.23	1.88	0.93	38.0	1449	291.3	71.9
30.0	0.594	11.65	1.88	0.93	42.6	1475	294.5	74.6
32.0	0.587	12.59	1.88	0.93	16.0	1498	290.2	80.6
36.0	0.522	13.64	1.88	0.93	30.1	1511	256.6	87.4
48.0	0.546	14.09	1.88	0.95	62.2	1543	263.7	91.3
50.0	0.555	16.25	1.88	0.862	21.3	1473	267.3	100.0

FIGURE 3. Energy dependence on the real and imaginary potential depths extracted from the OM calculations.

FIGURE 4. Comparison between experimental angular distributions (solid black circles) for ^{6}Li + ^{16}O elastic scattering and the theoretical calculations (solid blue curves) using DFOM at E_{lab} = 13.0, 20.0, 25.7, and 30.0 MeV.

We used the following formula: $q = 2k \sin(\theta_{c.m./2})$ for calculating momentum transfer, where k is the wavenumber. As shown in Fig. 6, the plotted data as a function of momentum transfer exhibit repeated dips at momentum transfers around $q = 0.63$, 1.4, and 1.6 fm^{-1}. Consequently, we should be able to show that the forward angle dips are produced by the same potential "real part"; and the differences between the cross-sections at different energies at larger momentum transfer (angles) are due to the differences in the absorption at the larger values.

The calculated CF potential discussed in Sec. 2 was then used to fit the experimental ^{6}Li + ^{16}O elastic scattering angular distributions using two approaches. In the first approach, namely, "CF1", the real part derived besed on CF and an imaginary potential -which was taken the same as those obtained from OM analysis- were used to reproduce the experimental data. The data analysis using the CF1 approach was performed only with one adjustable parameter N_{RCF} "renormalization factors for the real part of CF potential"; the potential thus had the following form:

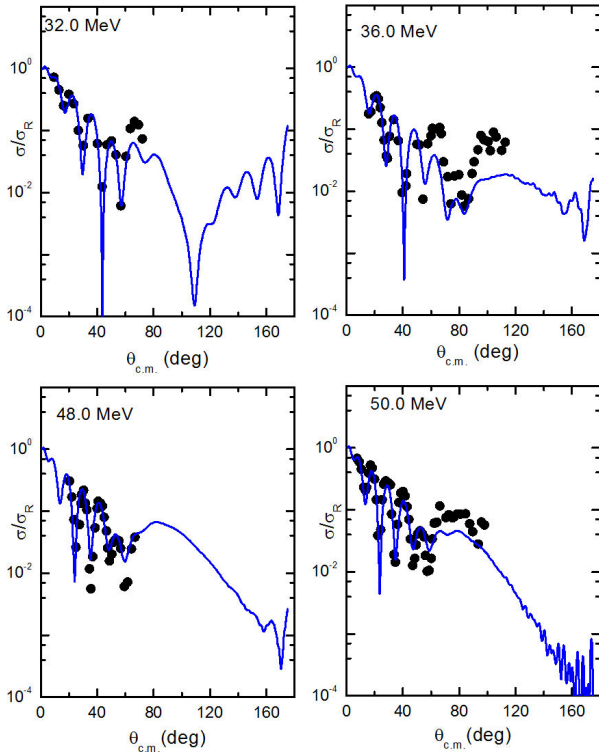$$U(r) = V_c(r) - N_{RCF}V_{CF}(r) - iWf(r, r_w, a_w), \quad (6)$$

FIGURE 5. Comparison between experimental angular distributions (solid black circles) for ^{6}Li + ^{16}O elastic scattering and the theoretical calculations (solid blue curves) using DFOM at $E_{lab} = 32.0, 36.0, 48.0,$ and 50.0 MeV.

The comparisons between the experimental angular distributions data for ^{6}Li + ^{16}O nuclear system at the different concerned energies and theoretical calculations using this CF1 approach are shown in Figs. 7-8. As shown in Table III, the value of N_{RCF} ranges between 1.01 and 1.05, and it is weakly dependent on bombarding energy.

In the second approach, namely, "CF2", the data were reproduced fully microscopically using only two adjustable parameters N_{RCF} and N_{ICF} "renormalization factors for the real and imaginary parts of CF potential"; the potential thus had the following form:

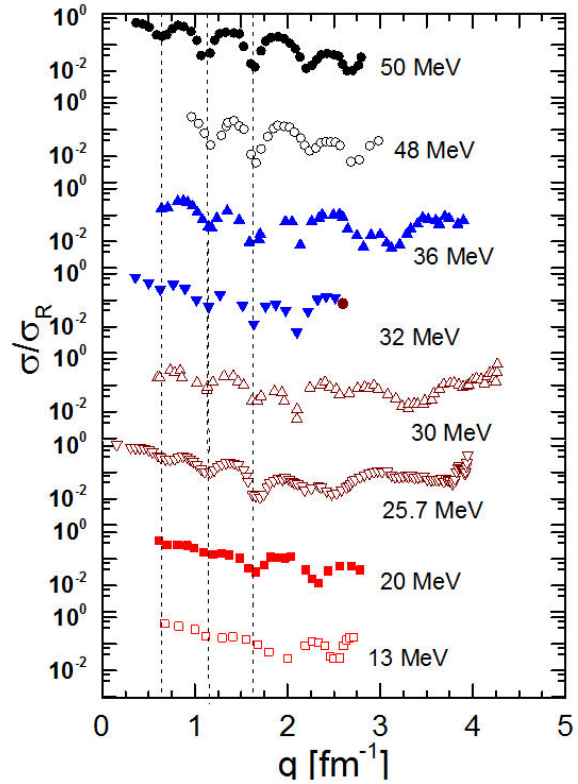$$U(r) = V_c(r) - N_{RCF}V_{CF}(r) - iN_{ICF}W_{CF}(r), \quad (7)$$

FIGURE 6. Experimental angular distributions for ^{6}Li + ^{16}O system plotted as a function of momentum transfer at energies $E_{lab} = 13.0, 20.0, 25.7, 30.0, 32.0, 36.0, 48.0,$ and 50.0 MeV.

TABLE III. Potential parameters for ^{6}Li + ^{16}O system extracted from CF1 approach, the values (σ_R, J_V and J_W) are also listed.

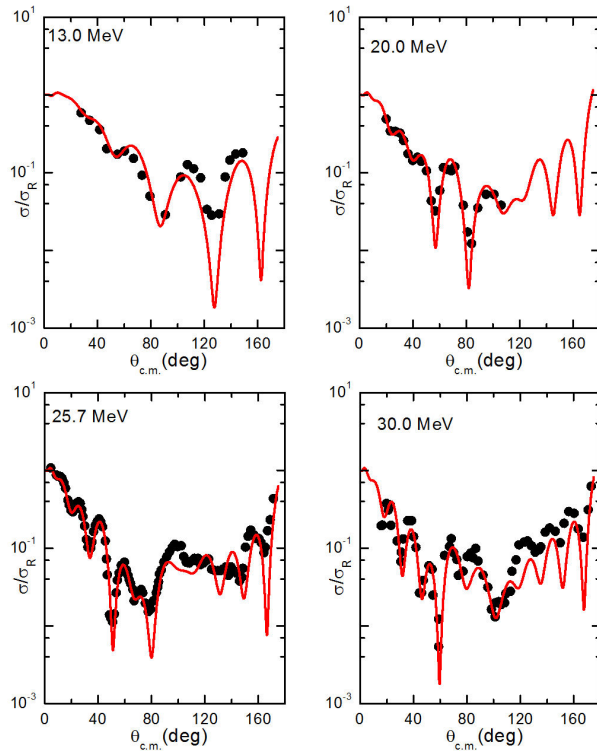| E | N_{RCF} | W_0 | r_W | a_W | χ^2/N | σ_R | J_V | J_W |
(MeV)		(MeV)	(fm)	(fm)		(mb)	(MeV.fm^3)	(MeV.fm^3)
13.0	1.05	7.14	1.88	0.949	18.3	1121	471.3	46.3
20.0	1.03	9.11	1.88	0.93	7.6	1310	462.4	58.3
25.7	1.04	11.23	1.88	0.93	12.8	1421	466.8	71.9
30.0	1.01	11.65	1.88	0.93	20.2	1448	453.4	74.6
32.0	1.02	12.59	1.88	0.93	15.4	1481	457.9	80.6
36.0	1.03	13.64	1.88	0.93	20.5	1511	462.4	87.4
48.0	1.05	14.09	1.88	0.95	42.2	1545	471.3	91.3
50.0	1.05	16.25	1.88	0.862	7.8	1477	471.3	100.0

FIGURE 7. Comparison between experimental angular distributions (solid black circles) for ^{6}Li + ^{16}O elastic scattering and the theoretical calculations (solid red curves) using CF1 approach at $E_{lab} = 13.0$, 20.0, 25.7, and 30.0 MeV.
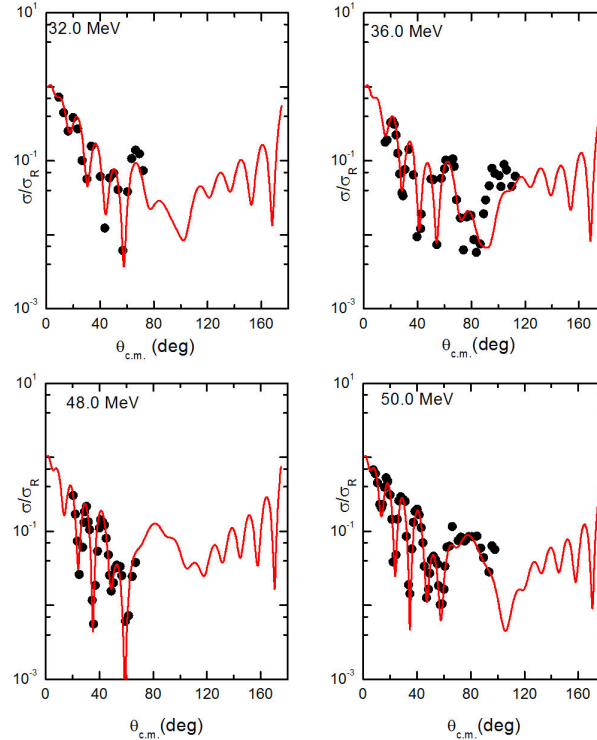

FIGURE 8. Comparison between experimental angular distributions (solid black circles) for ^{6}Li + ^{16}O elastic scattering and the theoretical calculations (solid red curves) using CF1 approach at $E_{lab} = 32.0$, 36.0, 48.0, and 50.0 MeV.
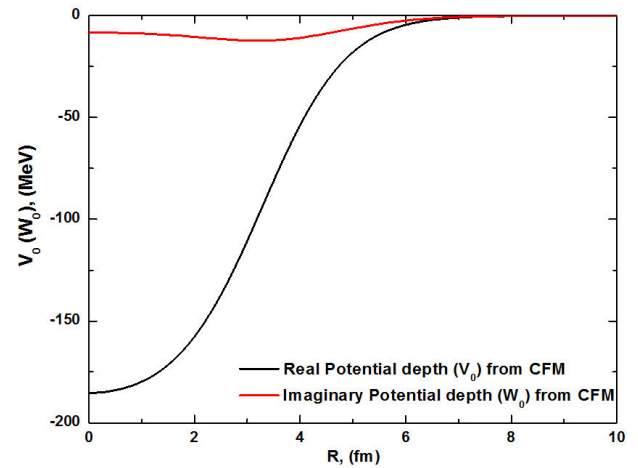

FIGURE 9. Variation in the real (V_0) and imaginary (W_0) potential depths derived from CF Model at different radii.
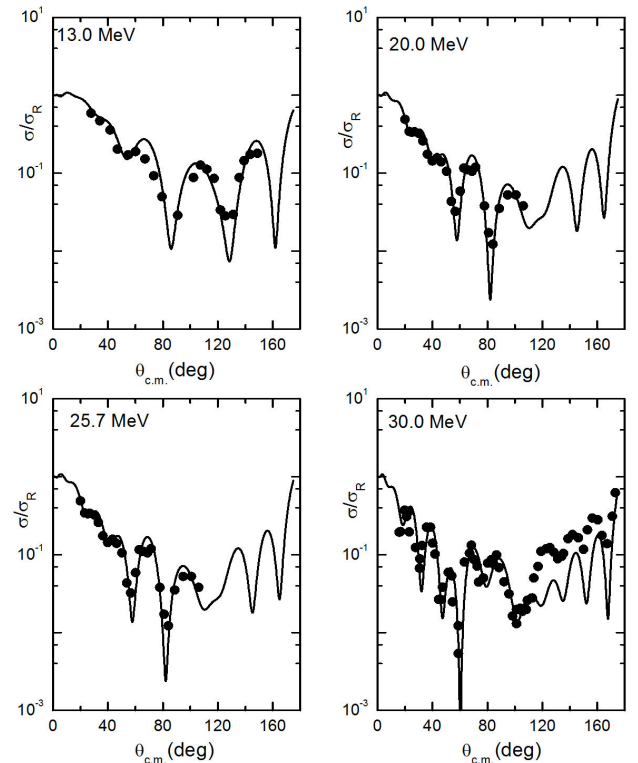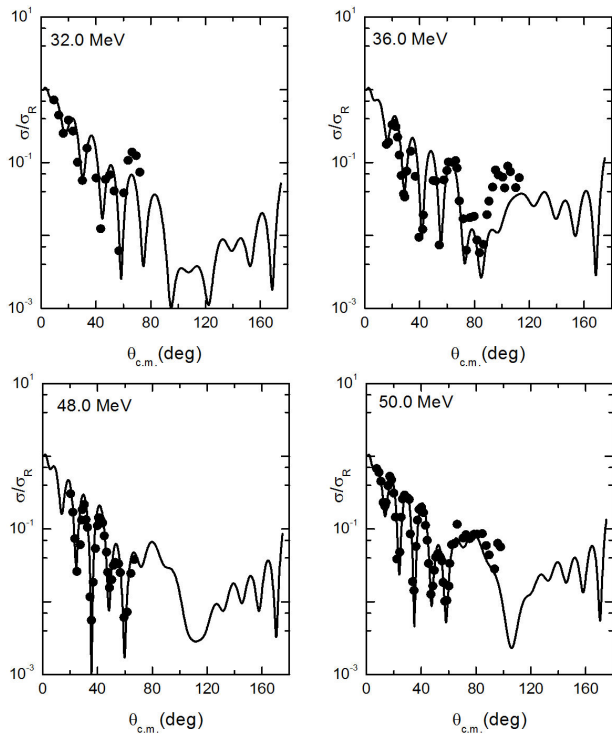

FIGURE 10. Comparison between experimental angular distributions (solid black circles) for the ^{6}Li + ^{16}O elastic scattering and the theoretical calculations (solid black curves) using CF2 approach at $E_{lab} = 13.0$, 20.0, 25.7, and 30.0 MeV.

The variation in cluster folding potential for both the real and imaginary parts with radius is shown in Fig. 9. The optimal values for N_{RCF} and N_{ICF} at different concerned energies were obtained by minimizing χ^2 using SFRESCO, the searching version of FRESCO. The best fit values are listed in Table IV. The comparisons between the experimental data and the theoretical calculations using the CF2 approach at different concerned energies are shown in Figs. 10-11. The

TABLE IV. Potential parameters for ^{6}Li + ^{16}O nuclear system extracted from CF2 approach, the values (σ_R, J_V and J_W) are also listed.

E (MeV)	N_{RCF}	N_{ICF}	χ^2/N	σ_R (mb)	J_V (MeV.fm^3)	J_W (MeV.fm^3)
13.0	1.06	0.58	15.9	972.5	475.8	48.5
20.0	1.04	0.75	11.1	1186	466.8	62.8
25.7	1.06	0.92	25.5	1279	475.8	77.0
30.0	1.03	0.92	31.5	1298	462.4	77.0
32.0	1.06	1.3	39.7	1375	475.8	108.8
36.0	1.03	1.15	60.1	1356	462.4	96.2
48.0	1.05	1.33	47.7	1397	471.3	111.3
50.0	1.05	1.27	14.7	1477	471.3	106.3

FIGURE 11. Comparison between experimental angular distributions (solid black circles) for the ^{6}Li + ^{16}O elastic scattering and the theoretical calculations (solid black curves) using CF2 approach at E_{lab} = 32.0, 36.0, 48.0, and 50.0 MeV.

4. Summary

The available experimental data for ^{6}Li + ^{16}O elastic scattering angular distributions in the energy range of 13.0-50.0 MeV were reanalyzed within the framework of different potentials: OM, DFOM, and CF potentials. The comparisons between the experimental data and theoretical calculations using the different concerned models were found to be fairly good. The data analysis using DFOM showed that the potentials needed to be reduced in strength by about 40%. This fact was also previously reported for various ^{6}Li +X nuclear systems [7]. The available data for ^{6}Li + ^{16}O system were plotted as a function of momentum transfer. In this case, the data exhibited repeated dips at momentum transfers at $q = 0.63$, 1.4, and 1.6 fm^{-1}. This means that the forward angle dips should be reproduced by the same potential "real part" and the differences between the cross-sections at different energies and larger angles are due to the differences in the absorption at the larger values. In the present work, we carried out further microscopic analysis of the ^{6}Li + ^{16}O elastic scattering based on the CF potential. We hope to minimize what are probably the largest sources of the model dependence of the extracted renormalization factor for this system. The renormalization factors of the real and imaginary parts of the CF optical potential were tuned to give the best agreement with the elastic scattering data. The data analysis using CF1 and CF2 approaches showed that the value of N_{RCF} is about 1.0, and it is weakly dependent on energy.

Acknowledgments

data analysis using the CF2 approach also showed that the value of N_{RCF} is weakly dependent on energy and ranges between 1.03 and 1.06, while N_{ICF} is strongly dependent on energy (Table IV). In other words and as shown in Fig. 6, the data at forwarding angles could be reproduced by the same potential "real part"; and the differences between the cross-sections at different energies and larger angles are due to the differences in the absorption at the larger values.

1. J. E. Poling, E. Norbeck, and R. R. Carlson, Elastic Scattering of Lithium by Carbon, *Phys. Rev. C* **5** (1972) 1819, https://doi.org/10.1103/PhysRevC.5.1819.

2. P. K. Bindal, K. Nagatani, M. J. Schneider, and P. D. Bond, Elastic and inelastic scattering of ^{6}Li on ^{12}C, *Phys. Rev. C* **9** (1974) 2154, https://doi.org/10.1103/PhysRevC.9.2154.

3. J. E. Poling, E. Norbeck, and R. R. Carlson, Elastic scattering of lithium by ^{9}Be, ^{10}B, ^{12}C, ^{13}C, ^{16}O, and ^{28}Si from 4 to 63 MeV, *Phys. Rev. C* **13** (1976) 648, https://doi.org/10.1103/PhysRevC.13.648.

4. W. Schmidt and U. Strohbusch, Optical-model analysis for ^{6}Li elastic scattering by ^{16}O at 20 MeV, *Nucl. Phys. A* **159** (1970) 104, https://doi.org/10.1016/0375-9474(70)90663-9.

5. K. Bethge, C. M. Fou, and R. W. Zurmühle, Elastic scattering of lithium nuclei, *Nucl. Phys. A* **123** (1969) 521, https://doi.org/10.1016/0375-9474(69)91001-X.

6. S. R. Mokhtar, A. A. Ibraheem, E. Abdel-Rahman, and M. El-Azab Farid, Investigation of the ^{6}Li + ^{40}Ca elastic scattering using different folding models, *Eur. Phys. J. A* **54** (2018) 235, https://doi.org/10.1140/epja/i2018-12663-6.

7. A. A. Ibraheem and M. Aygun, A Comprehensive Theoretical Analysis of ^{6,7}Li + ^{64}Zn Elastic Scattering in a Wide Angular Range Around the Coulomb Barrier, *Braz. J. Phys.* **46** (2016) 424, https://doi.org/10.1007/s13538-016-0424-5.

8. A. H. Al-Ghamdi and A. A. Ibraheem, Analysis of ^{6}Li Scattering at 240 MeV Using Different Nuclear Potentials, *Braz. J. Phys.* **46** (2016) 334, https://doi.org/10.1007/s13538-016-0407-6.

9. A. A. Ibraheem, Folding model calculations for ^{6}He+^{12}C elastic scattering, *Chin. Phys. C* **40** (2016) 034102, https://doi.org/10.1088/1674-1137/40/3/034102.

10. L.-Y. Hu, Y.-S. Song, Y.-W. Hou, and H.-L. Liu, The cluster folding model analysis for the elastic scattering of ^{6}Li and ^{6}He on ^{12}C, *Eur. Phys. J. A* **54** (2018) 230, https://doi.org/10.1140/epja/i2018-12668-1.

11. A. T. Rudchik et al., Energy dependence of the ^{6}Li + ^{16}O elastic scattering versus that of ^{7}Li + ^{16}O, *Eur. Phys. J. A* **49** (2013) 74, https://doi.org/10.1140/epja/i2013-13074-y.

12. A. T. Rudchik *et al.*, ^{6}Li(^{18}O, ^{17}O)^{7}Li reaction and comparison of ^{6,7}Li + ^{16,17,18}O potentials, *Nucl. Phys. A* **927** (2014) 209, https://doi.org/10.1016/j.nuclphysa.2014.04.018.

13. M. F. Vineyard, J. Cook, K. W. Kemper, and M. N. Stephens, Optical potentials for the elastic scattering of ^{6}Li + ^{12}C, ^{6}Li + ^{16}O, and ^{7}Li + ^{12}C, *Phys. Rev. C* **30** (1984) 916, https://doi.org/10.1103/PhysRevC.30.916.

14. D. E. Trcka, A. D. Frawley, K. W. Kemper, D. Robson, J. D. Fox, and E. G. Myers, Angular momentum dependent absorption in ^{6}Li scattering, *Phys. Rev. C* **41** (1990) 2134, https://doi.org/10.1103/PhysRevC.41.2134.

15. V. V. Davydov, B. G. Novatskii, A. A. Ogloblin, S. B. Sakuta, D. N. Stepanov, and V. I. Chuev, Elastic Scattering of ^{6}Li Ions, *Izv. Akad. Nauk SSSR Ser. Fiz.* **35** (1971) 2399 [*Bull. Acad. Sci. USSR Phys. Ser.* 35 (1972) 2176].

16. N. Anantaraman, H. W. Fulbright, and P. M. Stwertka, Variation of ground state α-particle strengths for sd- and fp-shell nuclei, *Phys. Rev. C* **22** (1980) 501, https://doi.org/10.1103/PhysRevC.22.501.

17. P. Schumacher, N. Ueta, H. H. Duhm, K.-I. Kubo, and W. J. Klages, Lithium elastic and inelastic scattering and lithium-induced single nucleon transfer reactions, *Nucl. Phys. A* **212** (1973) 573, https://doi.org/10.1016/0375-9474(73)90824-5.

18. J. Cook et al., Large-angle enhancements in the ^{16}O(^{6}Li, α)^{18}F reaction at 48 MeV, *Nucl. Phys. A* **415** (1984) 114, https://doi.org/10.1016/0375-9474(84)90602-X.

19. I. J. Thompson, Coupled reaction channels calculations in nuclear physics, *Comput. Phys. Rep.* **7** (1988) 167, https://doi.org/10.1016/0167-7977(88)90005-6.

20. I. I. Gontchar and M. V. Chushnyakova, A C-code for the double folding interaction potential of two spherical nuclei, *Comput. Phys. Commun.* **181** (2010) 168, https://doi.org/10.1016/j.cpc.2009.09.007.

21. G. R. Satchler and W. G. Love, Folding model potentials from realistic interactions for heavy-ion scattering, *Phys. Rep.* **55** (1979) 183, https://doi.org/10.1016/0370-1573(79)90081-4.

22. S. Qing-biao, F. Da-chun, and Z. Yi-zhong, Neutron relativistic phenomenological and microscopic optical potential, *Phys. Rev. C* **43** (1991) 2773, https://doi.org/10.1103/PhysRevC.43.2773.

23. K. H. Bray et al., Elastic and inelastic scattering of protons from ^{6}Li between 25 and 45 MeV, *Nucl. Phys. A* **189** (1972) 35, https://doi.org/10.1016/0375-9474(72)90645-8.

24. A. A. Cowley, G. Heymann, R. L. Keizer, and M. J. Scott, Elastic and inelastic scattering of 15.8 MeV deuterons, *Nucl. Phys.* **86** (1966) 363, https://doi.org/10.1016/0029-5582(66)90544-X; C. M. Perey and F. G. Perey, Compilation of phenomenological optical-model parameters 1954-1975, *At. Data Nucl. Data Tables* **17** (1976) 1, https://doi.org/10.1016/0092-640X(76)90007-3.

25. A. A. Cowley, G. Heymann, Regge pole analysis of the elastic scattering of α-particles from ^{16}O, *Nucl. Phys. A* **146** (1970) 465, https://doi.org/10.1016/0375-9474(70)90740-2.